ACCSCIENCE PUBLISHING

Journal of Seismic Exploration

ARTICLE

Seismic prediction methods for evaluating *in situ* stress in tilted transversely isotropic and monoclinic media

Jun Cheng[1], Yaojie Chen[2]*, and Zhensen Sun[3]

[1]Petroleum Development Center, Shengli Oilfield, Sinopec, Dongying, Shandong, China

[2]Department of Geophysical Exploration, School of Geoscience and Technology, Southwest Petroleum University, Chengdu, Sichuan, China

[3]Nanhai East Petroleum Research Institute, Shenzhen Branch, China National Offshore Oil Corporation Ltd., Shenzhen, Guangdong, China

Abstract

The formation of tectonic fractures is primarily influenced by stress distribution during the tectonic period. Therefore, *in situ* stress plays a crucial role in predicting fracture development zones. It significantly impacts the effectiveness of fractures by determining the size, orientation, and distribution pattern of fractures, thereby affecting stimulation results. Existing seismic methods for *in situ* stress prediction utilize seismic data to estimate stress parameters and calculate the horizontal stress difference ratio or the orthorhombic horizontal stress difference ratio (DHSR). These methods are based on the horizontal transverse isotropy or the orthorhombic anisotropy medium models. However, shale formations are often subject to tectonic movements that can rotate the symmetry axis of a transversely isotropic medium, leading to the formation of a tilted transversely isotropic (TTI) medium or a monoclinic medium with an inclined symmetry plane. Based on the TTI and monoclinic medium assumptions, this paper proposes new formulas for calculating the DHSRs (tilted transverse isotropy DHSR and monoclinic DHSR). The formulas are further validated through sensitivity analyses. Finally, this study demonstrates the effectiveness of the *in situ* stress seismic prediction method, grounded in TTI, and monoclinic medium theory through model-based examples.

Keywords: *In situ* stress; Tilted transverse isotropy differential horizontal stress ratio; Monoclinic differential horizontal stress ratio

***Corresponding author:**
Yaojie Chen
(202311000091@stu.swpu.edu.cn)

Citation: Cheng J, Chen Y, Sun Z. Seismic prediction methods for evaluating *in situ* stress in tilted transversely isotropic and monoclinic media. *J Seismic Explor.* 2025;34(1): 60-80.
doi: 10.36922/JSE025190002

Received: May 9, 2025

1st revised: July 3, 2025

2nd revised: July 22, 2025

3rd revised: August 1, 2025

Accepted: August 1, 2025

Published online: August 15, 2025

1. Introduction

With the growing global demand for energy, shale gas has garnered significant attention as a clean and efficient energy resource. In the exploration and development of shale gas reservoirs, *in situ* stress prediction plays a critical role. *In situ* stress, carried by underground rocks and pore fluids, is crucial for effective oil and gas exploration. The influence of tectonic stress drives the formation and evolution of geological structures. Furthermore, the *in situ* stress state of an oilfield governs the shape and distribution of faults. Therefore, studying *in situ* stress is essential for understanding geological structure formation and fault distribution. In-depth research on *in situ* stress prediction methods

for shale formations is vital for advancing the sustainable development of the shale gas industry.

Since the 1970s, both domestic and international scholars have conducted extensive research on methods for predicting *in situ* stress. Traditional methods, such as core testing, logging data analysis, and numerical simulations, have certain limitations, including small prediction ranges, high costs, and cumbersome processes. To better understand the nature and changes of *in situ* stress, researchers have proposed using seismic data for prediction.[1-4] In this context, Gray *et al.*[5] combined Iverson's hypothesis with linear slip theory to derive a horizontally transversely isotropic (HTI) medium *in situ* stress formula, which incorporates parameters such as Young's modulus, Poisson's ratio, and fracture compliance.[5-8] Given that these parameters can be directly obtained through pre-stack seismic inversion, this approach has become a promising direction for seismic *in situ* stress prediction.[9,10] In addition, Gray[7] introduced the horizontal stress difference ratio (DHSR) as the ratio of the difference between the maximum and minimum horizontal principal stresses to the maximum principal stress, providing a new way to describe ground stress. Unlike traditional methods, this approach is simple and practical. It addresses the challenge of inaccurate vertical stress prediction caused by the low accuracy of density inversion using DHSR as a sensitive *in situ* stress parameter. Compared to traditional logging-based methods, which are limited to drilling locations and suffer from low lateral resolution, this seismic method can provide *in situ* stress distributions across large areas, offering a more comprehensive understanding of underground stress and better guidance for petroleum engineering. Gray's method thus introduces a novel approach and practical tool to *in situ* stress research, greatly supporting fields such as petroleum exploration and development.

Building on Gray's work, Ma *et al.*[11,12] incorporated vertical fractures into the vertically transversely isotropic (VTI) medium for horizontal layered strata, treating fractured shale formations as orthotropic media. Using anisotropic media theory, they derived an orthotropic *in situ* stress formula. Following Gray's concept of the DHSR, they introduced the orthorhombic DHSR for the orthorhombic anisotropy (OA) medium. Wang[13] used azimuth-pre-stack seismic data combined with orthogonal anisotropy theory to predict ground stress, while also calculating the DHSR from the orthogonal anisotropy model combined with pre-stack elastic impedance inversion, focusing on tight sandstone formations.[14] Li *et al.*[15] utilized seismic inversion to estimate intercept, gradient, and curvature impedances to predict ground stress.[15] In addition, Wang *et al.*[16] proposed an inversion algorithm for the earth stress field based on the Tikhonov regularization and least squares methods.[16] Geophysical prediction methods are subject to significant uncertainty. This is primarily because seismic inversion is a typical ill-posed problem, and seismic data are often affected by noise, which leads to considerable uncertainty in *in situ* stress prediction. Researchers have conducted studies to reduce the uncertainty associated with these prediction methods.[17-22] However, as geophysical theories advance and our understanding of underground rock conditions deepens, there is a shift from modeling simple media to more complex media. Given the increasing complexity of real-world factors, it is essential to explore *in situ* stress characterization methods for these more complex media.

Formations comprising inclined fractures are widely distributed underground and can be effectively represented as tilted transversely isotropic (TTI) media. Vertically transversely isotropic (VTI) symmetry is most commonly found in shale formations, which account for approximately 75% of clastic infill in sedimentary basins worldwide. However, in tectonically active regions such as fold-and-thrust belts or areas near salt bodies, these anisotropic shale layers are often tilted due to structural deformation, resulting in TTI media. For example, up-dipping shale layers near salt domes are expected to form an effective TTI medium with a relatively large tilt of the symmetry axis. TTI models are also typically applicable to thrust fault zones, such as the Canadian Foothills or the Himalayan Foothills. TI shale layers are frequently bent by tectonic processes, often resulting in significant tilting.[23,24] In 1997, Tsvankin[25] studied typical TI models with tilted symmetry axes, such as sediments near the flanks of salt domes, and found that dipping layers significantly affect the imaging of salt bodies. When imaging steeply dipping structures such as salt domes or volcanic intrusions, the tilt of the symmetry axis in TI media should be taken into account.[25] In 2004, Isaac and Lawton[26] proposed an independent method for estimating effective anisotropic parameters from surface P-wave reflection seismic data. They tested this approach using a two-dimensional physical model of seismic data from a stepped target beneath a tilted TTI overburden. The experimental results showed that assuming isotropy in an equivalent TTI medium led to significant errors, thereby demonstrating the impact of anisotropy.[26] In 2008, Charles *et al.*[27] studied seismic imaging in the Canadian Foothills thrust belt. In the study area, the shallow overburden was composed of tilted, shale-dominated clastic rocks, which exhibited weak TTI properties. The experimental results showed that anisotropic depth imaging based on data-driven tomography produced better results than isotropic depth imaging using the same tomography approach.[27] In many

cases, formations subjected to either single-phase shear stress or multiple tectonic events tend to develop two sets of mutually oblique vertical fractures. Such formations can be abstracted in seismology as a special case of monoclinic anisotropic media. Reservoirs with monoclinic symmetry are quite common in oil and gas exploration. Examples include the Ordovician formations in the Tofutai area of the Tarim Basin in China,[28] the carbonate formations of the Clair Group in the Clair Field, United Kingdom,[29] and the Marcellus Shale in Bradford County, Pennsylvania, United States of America,[30] all of which represent monoclinic reservoirs with hydrocarbon potential. In 2023, Li[31] conducted a seismic response analysis and parameter inversion for a monoclinic medium model induced by two sets of mutually oblique vertical fractures. The study area was located in the Sichuan Basin in southwestern China, where the reservoir belongs to the Lower Triassic and is characterized by well-developed tectonic fractures due to the influence of the Himalayan orogeny. During the Triassic compressional period, one set of extensional fractures formed concurrently with folding. Subsequently, during the Himalayan orogenic phase, renewed compressional stress acted on the pre-existing folds, resulting in the development of a second set of fractures. This led to the formation of an equivalent monoclinic anisotropic medium. The inversion method was ultimately applied to the study area, improving the accuracy of the inversion results.[31] These cases clearly demonstrate the necessity of incorporating the effects of TTI and monoclinic anisotropy in seismic stress field prediction for geologically complex regions. Neglecting such anisotropy may lead to misinterpretations of fracture orientation, stress magnitude, and the geomechanical behavior of the reservoir. Therefore, research on stress field prediction based on TTI and monoclinic media is of critical importance.

Considering that inclined fractures influence actual shale formations, this study proposes *in situ* stress formulas based on the TTI and monoclinic media, along with the corresponding DHSRs, including the tilted transverse isotropy DHSR (TDHSR) and the monoclinic DHSR (MDHSR). By fully accounting for the effects of horizontal bedding and inclined fractures on DHSRs, the derived expressions offer higher applicability than the HTI and OA media, allowing for more accurate application to complex TTI and monoclinic media. This provides a more robust theoretical foundation for related research and applications.

First, the *in situ* stress formulas for the HTI and OA media are introduced. Then, based on the anisotropy theory, the formulas for the DHSRs in TTI and monoclinic media are derived. The correctness of these formulas is verified through formula degradation and model trial calculations. Finally, the relationship between the DHSRs of TTI and monoclinic media and factors such as elastic parameters, anisotropy parameters, and the dip angles of formations and fractures is analyzed and summarized. Model-based analysis further demonstrates the validity of the *in situ* stress seismic prediction method based on the TTI and monoclinic medium theories.

2. Materials and methods

2.1. Introduction to the basic theory

The constitutive equation of an elastic medium is an equation that describes the linear relationship between stress and strain using the stiffness tensor, also known as the generalized Hooke's law. For any anisotropic linear elastic medium, the stress and strain have the following linear relationship in **Equation I**:

$$\sigma_{ij} = C_{ijkl}\varepsilon_{kl}(\mathrm{i,j,k,l} \in 1,2,3) \tag{I}$$

where σ_{ij} is the stress tensor, ε_{kl} is the strain tensor, and C_{ijkl} is the stiffness tensor. Conversely, strain can also be expressed as a linear combination of stresses (**Equation II**):

$$\varepsilon_{ij} = S_{ijkl}\sigma_{kl}(\mathrm{i,j,k,l} \in 1,2,3) \tag{II}$$

where S_{ijkl} is the elastic compliance tensor (compliance matrix). The compliance matrix S and the stiffness matrix C have an inverse matrix relationship, and the expression of their mutual conversion is as follows (**Equation III**):

$$S = C^{-1} \tag{III}$$

The subscript i,j,k,l = 1,2,3 of the elastic stiffness tensor C_{ijkl} or the elastic compliance tensor S_{ijkl} corresponds to the x, y, and z axes. Combining the number of subscripts and the number of symmetry axes subscripts, it can be seen that the fourth-order stiffness tensor and the compliance tensor contain 81 elements, and the second-order stress tensor σ_{ij} and strain tensor C_{ijkl} contain nine elements. The inherent symmetry of stress tensor and strain tensor causes the stiffness matrix to exhibit symmetric characteristics (**Equation IV**),

$$C_{ijkl} = C_{jikl} = C_{jilk} = C_{jilk} \tag{IV}$$

According to the symmetry of the stiffness matrix in Equation V:

$$C_{ijkl} = C_{klij} \tag{V}$$

Therefore, by combining Equations IV and V, the anisotropic stiffness matrix can be represented by 21 independent elastic coefficients. The stiffness matrix C_{ijkl} (i,j,k,l=1,2,3) can be transformed into the stiffness matrix of i,j = 1,2,3,4,5,6, and the stress and strain tensors can be transformed into σ_i and ε_j by using the Voigt notation. Table 1 lists the Voight conversion rules.

Equations I and **II** then transform into **Equations VI** and **VII**:

$$\sigma_i = C_{ij}\varepsilon_j (i,j \in 1,2,\cdots,6) \quad \text{(VI)}$$

$$\varepsilon_i = S_{ij}\sigma_j (i,j \in 1,2,\cdots,6) \quad \text{(VII)}$$

The elastic matrix describing the relationship between stress and strain changes from 81 components to 21 independent components. Hence, the constitutive equation of the elastic matrix can be written as follows (**Equation VIII**):

$$\begin{bmatrix}\sigma_1\\ \sigma_2\\ \sigma_3\\ \sigma_4\\ \sigma_5\\ \sigma_6\end{bmatrix} = \begin{bmatrix}C_{11} & C_{12} & C_{13} & C_{14} & C_{15} & C_{16}\\ C_{12} & C_{22} & C_{23} & C_{24} & C_{25} & C_{26}\\ C_{13} & C_{23} & C_{33} & C_{34} & C_{35} & C_{36}\\ C_{14} & C_{24} & C_{34} & C_{44} & C_{45} & C_{46}\\ C_{15} & C_{25} & C_{35} & C_{45} & C_{55} & C_{56}\\ C_{16} & C_{26} & C_{36} & C_{46} & C_{56} & C_{66}\end{bmatrix}\begin{bmatrix}\varepsilon_1\\ \varepsilon_2\\ \varepsilon_3\\ \varepsilon_4\\ \varepsilon_5\\ \varepsilon_6\end{bmatrix} \quad \text{(VIII)}$$

The stiffness matrix in Equation VIII contains 21 elastic constants, which are generally considered independent in fully anisotropic media. However, in many cases, several elements of the stiffness matrix are either zero or constrained by symmetry. Moreover, not all nonzero stiffness elements are necessarily independent—for example, in transversely isotropic media. Typically, the greater the number of zero or constrained elements, the higher the degree of inherent symmetry in the elastic system of the medium.

The study of the elastic matrix in anisotropic media is typically conducted within the context of a constitutive coordinate system. However, due to the actual stratigraphic conditions, the constitutive coordinate system used for simulating complex anisotropic media may not align with the observed coordinate system. Therefore, a coordinate transformation is needed to unify elastic matrices across different coordinate systems. In the anisotropic media theory, the classification of anisotropic media is based on the angle between the medium's symmetry axis and the observation coordinate system.

Table 1. Voigt symbol conversion rules

Values for *ij* or *kl*	Values for *i* or *j*
11	1
22	2
33	3
23 or 32	4
31 or 13	5
12 or 21	6

Two steps are typically required to transform a complex anisotropic medium into the observation coordinate system. First, the stiffness tensor is constructed in the material (constitutive) coordinate system. Then, a Bond transformation is applied to rotate the stiffness tensor into the observation coordinate system. It is important to note that the Bond transformation strictly applies to the fourth-rank stiffness tensor, not to the 6 × 6 stiffness matrix obtained using Voigt's notation. This coordinate transformation process is essential for accurately representing anisotropic media in complex stratigraphic settings.

Assuming that the observation coordinate system and the constitutive coordinate system are *Oxyz* and *Ox'y'z'*, respectively, the direction cosine relationship between the observation coordinate system and the constitutive coordinate system (coordinate axis) in the Bond transformation is shown in Table 2.

Assuming that the stress tensor, strain tensor, stiffness matrix, and compliance matrix under the observation coordinate system and the constitutive coordinate system are σ, ε, C, and S and σ', ε', C', and S', respectively, according to the Bond coordinate transformation, the stress and strain transformation under different coordinate systems can be expressed as **Equations IX–XI**:

$$\sigma = M \cdot \sigma' \quad \text{(IX)}$$

$$\varepsilon = M^T \cdot \varepsilon' \quad \text{(X)}$$

$$M = \begin{bmatrix}\alpha_1^2 & \beta_1^2 & \gamma_1^2 & 2\beta_1\gamma_1 & 2\alpha_1\gamma_1 & 2\alpha_1\beta_1\\ \alpha_2^2 & \beta_2^2 & \gamma_2^2 & 2\beta_2\gamma_2 & 2\alpha_2\gamma_2 & 2\alpha_2\beta_2\\ \alpha_3^2 & \beta_3^2 & \gamma_3^2 & 2\beta_3\gamma_3 & 2\alpha_3\gamma_3 & 2\alpha_3\beta_3\\ \alpha_2\alpha_3 & \beta_2\beta_3 & \gamma_2\gamma_3 & \beta_2\gamma_3+\beta_3\gamma_2 & \gamma_2\alpha_3+\gamma_3\alpha_2 & \alpha_2\beta_3+\alpha_3\beta_2\\ \alpha_1\alpha_3 & \beta_1\beta_3 & \gamma_1\gamma_3 & \beta_1\gamma_3+\beta_3\gamma_1 & \gamma_1\alpha_3+\gamma_3\alpha_1 & \alpha_1\beta_3+\alpha_3\beta_1\\ \alpha_1\alpha_2 & \beta_1\beta_2 & \gamma_1\gamma_2 & \beta_1\gamma_2+\beta_2\gamma_1 & \gamma_1\alpha_2+\gamma_2\alpha_1 & \alpha_1\beta_2+\alpha_2\beta_1\end{bmatrix} \quad \text{(XI)}$$

Through derivation, we can get **Equation XII**:

$$\sigma = M \cdot C' \cdot M^T \cdot \varepsilon \quad \text{(XII)}$$

The stiffness matrix constitutive equation can be used to obtain **Equation XIII**:

$$C = M \cdot C' \cdot M^T \quad \text{(XIII)}$$

Table 2. The direction cosine relationship between the observation and the constitutive coordinate system (axis)

Axis	*x'*	*y'*	*z'*
x	α_1	β_1	γ_1
y	α_2	β_2	γ_2
z	α_3	β_3	γ_3

Similarly, the relationship between strain and stress is as follows (**Equations XIV–XVI**):

$$\sigma = N^T \cdot \sigma' \qquad \text{(XIV)}$$

$$\varepsilon = N \cdot \varepsilon' \qquad \text{(XV)}$$

$$N = \begin{bmatrix} \alpha_1^2 & \beta_1^2 & \gamma_1^2 & \beta_1\gamma_1 & \alpha_1\gamma_1 & \alpha_1\beta_1 \\ \alpha_2^2 & \beta_2^2 & \gamma_2^2 & \beta_2\gamma_2 & \alpha_2\gamma_2 & \alpha_2\beta_2 \\ \alpha_3^2 & \beta_3^2 & \gamma_3^2 & \beta_3\gamma_3 & \alpha_3\gamma_3 & \alpha_3\beta_3 \\ 2\alpha_2\alpha_3 & 2\beta_2\beta_3 & 2\gamma_2\gamma_3 & \beta_2\gamma_3+\beta_3\gamma_2 & \gamma_2\alpha_3+\gamma_3\alpha_2 & \alpha_2\beta_3+\alpha_3\beta_2 \\ 2\alpha_1\alpha_3 & 2\beta_1\beta_3 & 2\gamma_1\gamma_3 & \beta_1\gamma_3+\beta_3\gamma_1 & \gamma_1\alpha_3+\gamma_3\alpha_1 & \alpha_1\beta_3+\alpha_3\beta_1 \\ 2\alpha_1\alpha_2 & 2\beta_1\beta_2 & 2\gamma_1\gamma_2 & \beta_1\gamma_2+\beta_2\gamma_1 & \gamma_1\alpha_2+\gamma_2\alpha_1 & \alpha_1\beta_2+\alpha_2\beta_1 \end{bmatrix} \qquad \text{(XVI)}$$

Through derivation, we can get **Equation XVII**:

$$\varepsilon = N \cdot S^{'} \cdot N^T \cdot \sigma \qquad \text{(XVII)}$$

The stiffness matrix constitutive equation can be used to obtain **Equation XVIII**:

$$S = N \cdot S^{'} \cdot N^T \qquad \text{(XVIII)}$$

The matrices M and N are the Bond transformation matrices of the stiffness matrix and the compliance matrix, respectively, and T represents the transpose.

2.2. Derivation of the *in situ* stress formula for the TTI medium

In 1989, Crampin[1] classified various anisotropic media by analyzing their stiffness matrices and the number of independent elastic parameters, based on the symmetry of the medium. Isotropy refers to a medium whose elastic properties are the same in all directions and do not change with the direction of wave propagation. It is the simplest type of medium and can be considered a special case of anisotropy. While the complete isotropic medium is a simplification for geophysical research, real underground media are composed of superimposed lithologic strata, where the same strata exhibit uniform geophysical properties, thus behaving isotropically.

In anisotropic media theory, a TI medium exhibits rotational symmetry about a single axis. In such media, the material properties are isotropic within the plane perpendicular to the symmetry axis—known as the isotropy plane—and vary only with the angle between the wave propagation direction and the symmetry axis.[32,33] TI media can be further classified based on the direction of the symmetry axis into VTI media (vertical symmetry axis), HTI media (horizontal symmetry axis), and TTI media (tilted symmetry axis). Figure 1 illustrates a schematic of TI media, which have different symmetry axes and can be transformed into one another through rotation.

Although most natural fractures are vertical or subvertical, tectonic processes can result in fractures that are inclined at an angle to the stratigraphy. Monoclinic media are typically used to describe scenarios involving two sets of intersecting vertical fractures embedded in a VTI or isotropic background (Figure 2A and B), or a VTI background containing a single set of inclined fractures (Figure 2C).

In a TTI medium, the anisotropy can be regarded as a result of the rotation of either a VTI or an HTI medium by a certain angle. The stiffness (or compliance) properties of a TTI medium are obtained by applying the Bond transformation to the fourth-rank stiffness (or compliance) tensor of the corresponding VTI or HTI medium. It should be noted that

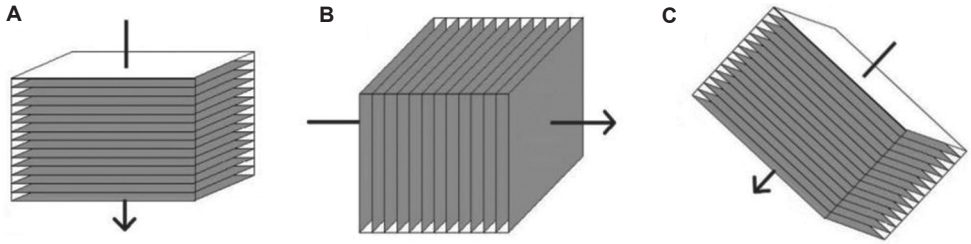

Figure 1. Diagram of the transversely isotropic media. (A) Vertically transversely isotropic medium, (B) horizontally transversely isotropic medium, and (C) tilted transversely isotropic medium

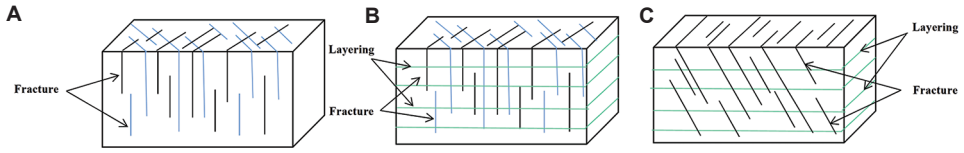

Figure 2. Diagram of monoclinic media. (A) Two groups of intersecting vertical fracture groups developed in an isotropic background medium. (B) Two groups of intersecting vertical fracture groups developed in a vertically transversely isotropic (VTI) background medium. (C) A group of inclined fractures developed in the VTI background media

the Bond transformation applies to the full tensor, not to the 6×6 matrix representation used in Voigt's notation.

In the subsequent derivation of this paper, the TTI medium is assumed to be formed by rotating a VTI medium. According to the definition of the linear slip model, when fractures develop horizontally (i.e., when the symmetry axis is vertical), the compliance tensor of the surrounding rock S_b can be expressed in terms of Young's modulus E and Poisson's ratio v as follows (**Equation XIX**):

$$S_b = \begin{pmatrix} \frac{1}{E} & \frac{-v}{E} & \frac{-v}{E} & 0 & 0 & 0 \\ \frac{-v}{E} & \frac{1}{E} & \frac{-v}{E} & 0 & 0 & 0 \\ \frac{-v}{E} & \frac{-v}{E} & \frac{1}{E} & 0 & 0 & 0 \\ 0 & 0 & 0 & \frac{1}{\mu} & 0 & 0 \\ 0 & 0 & 0 & 0 & \frac{1}{\mu} & 0 \\ 0 & 0 & 0 & 0 & 0 & \frac{1}{\mu} \end{pmatrix}_{6\times6} \quad \text{(XIX)}$$

where μ is the Lamé coefficient, which characterizes the rock's resistance to shear deformation. The additional compliance tensor S_f caused by fractures can be expressed as **Equation XX**:

$$S_f = \begin{pmatrix} 0 & 0 & 0 & 0 & 0 & 0 \\ 0 & 0 & 0 & 0 & 0 & 0 \\ 0 & 0 & Z_N & 0 & 0 & 0 \\ 0 & 0 & 0 & Z_T & 0 & 0 \\ 0 & 0 & 0 & 0 & Z_T & 0 \\ 0 & 0 & 0 & 0 & 0 & 0 \end{pmatrix}_{6\times6} \quad \text{(XX)}$$

where, Z_N is the normal compliance tensor of the fracture surface, representing the unit normal displacement (deformation) caused by a unit normal stress. Z_T is the tangential compliance tensor of the fracture surface, representing the unit tangential displacement caused by a unit tangential stress (parallel to the contact surface). By incorporating the linear slip theory and the Bond transformation, the effective compliance tensor of the TTI medium, S_T, can be expressed as the sum of the compliance tensor of the rock skeleton, S_b, and the compliance tensor of microcracks in the rock, S_f, after applying the Bond transformation. Thus, the effective compliance tensor of the TTI medium, S_T, can be written as **Equations XXI** and **XXII (see page no 20)**:

$$S_T = S_b + N_\theta S_f N_\theta^T \quad \text{(XXI)}$$

Substituting the compliance matrix of TTI medium into Hooke's law can result in **Equation XXIII**:

$$\begin{bmatrix} \varepsilon_1 \\ \varepsilon_2 \\ \varepsilon_3 \\ \varepsilon_4 \\ \varepsilon_5 \\ \varepsilon_6 \end{bmatrix} = \begin{bmatrix} S_{11t} & S_{12t} & S_{13t} & 0 & S_{15t} & 0 \\ S_{21t} & S_{22t} & S_{23t} & 0 & S_{25t} & 0 \\ S_{31t} & S_{32t} & S_{33t} & 0 & S_{35t} & 0 \\ 0 & 0 & 0 & S_{44t} & 0 & S_{46t} \\ S_{51t} & S_{52t} & S_{53t} & 0 & S_{55t} & 0 \\ 0 & 0 & 0 & S_{64t} & 0 & S_{66t} \end{bmatrix} \begin{bmatrix} \sigma_1 \\ \sigma_2 \\ \sigma_3 \\ \sigma_4 \\ \sigma_5 \\ \sigma_6 \end{bmatrix} \quad \text{(XXIII)}$$

Among them, S_{ijt} is the elastic compliance tensor of the TTI medium. σ_1, σ_2, and σ_3 the principal stresses are in the three principal directions. σ_4, σ_5, and σ_6 are shear stresses.

Iverson's theory states that there are vertical principal stress and two horizontal stresses in anisotropic rocks.[34] Assuming that the horizontal stresses are not equal and assuming that the underground rocks are constrained, that is, they are immobile, then the horizontal strain (ε_x, ε_y) is equal to zero. According to **Equation XXIII**, the expression of strain and stress in the horizontal direction is expressed in **Equations XXIV** and **XXV**:

$$\varepsilon_x = \varepsilon_1 = S_{11t}\sigma_x + S_{12t}\sigma_y + S_{13t}\sigma_z + S_{15t}\sigma_{zx} = 0 \quad \text{(XXIV)}$$

$$\varepsilon_y = \varepsilon_2 = S_{21t}\sigma_x + S_{22t}\sigma_y + S_{23t}\sigma_z + S_{25t}\sigma_{zx} = 0 \quad \text{(XXV)}$$

In *in situ* stress prediction, researchers typically consider only the three principal stresses: vertical stress, minimum horizontal principal stress, and maximum horizontal principal stress. Therefore, this paper disregards the influence of tangential stress σ_5 and focuses solely on the relationship among these three principal stresses. The final expressions for strain and stress in the horizontal direction are expressed in **Equations XXVI** and **XXVII**:

$$\varepsilon_x = \varepsilon_1 = S_{11t}\sigma_x + S_{12t}\sigma_y + S_{13t}\sigma_z = 0 \quad \text{(XXVI)}$$

$$\varepsilon_y = \varepsilon_2 = S_{21t}\sigma_x + S_{22t}\sigma_y + S_{23t}\sigma_z = 0 \quad \text{(XXVII)}$$

By solving equations through simultaneous equations, the expressions for the horizontal minimum principal stress σ_{xt} and horizontal maximum principal stress σ_{yt} of TTI medium can be obtained (**Equations XXVIII** and **XXIX**):

$$\sigma_{xt} = \sigma_z \frac{S_{12t}S_{23t} - S_{13t}S_{22t}}{S_{11t}S_{22t} - S_{12t}^2} \quad \text{(XXVIII)}$$

$$\sigma_{yt} = \sigma_z \frac{S_{12t}S_{13t} - S_{11t}S_{23t}}{S_{11t}S_{22t} - S_{12t}^2} \quad \text{(XXIX)}$$

The vertical stress σ_z is obtained by integrating the density. The expression for vertical stress σ_z is expressed in **Equation XXX**:

$$\sigma_z = \int_0^H g\rho(\mathrm{h})\,\mathrm{d}(\mathrm{h}) \quad \text{(XXX)}$$

In the formula, h is the depth, g is the gravitational acceleration, and p (h) is the density at depth.

Bringing the constant term of the compliance matrix into it yields the corresponding stress expressions in **Equations XXXI** and **XXXII**:

$$\sigma_{xt} = \sigma_z \left(\frac{\upsilon + \upsilon^2 + \frac{1}{4}E\left(Z_T - Z_N\right)\sin^2(2\theta)}{1 - \upsilon^2 + EZ_N \sin^4(\theta) + \frac{1}{4}EZ_T \sin^2(2\theta)} \right) \quad \text{(XXXI)}$$

$$\sigma_{yt} = \sigma_z \upsilon \left(\frac{1 + \upsilon - EZ_N\left(\frac{1}{4}\sin^2(2\theta) - \sin^4(\theta)\right) + \frac{1}{2}EZ_T \sin^2(2\theta)}{1 - \upsilon^2 + EZ_N \sin^4(\theta) + \frac{1}{4}EZ_T \sin^2(2\theta)} \right) \quad \text{(XXXII)}$$

The vertical stress σ_z can be estimated using seismic or logging data. By integrating the pre-stack wide-azimuth seismic inversion to derive elastic and anisotropic parameters and then substituting them into **Equations XXXI** and **XXXII**, the horizontal minimum principal stress and horizontal maximum principal stress of the TTI medium can be predicted. Furthermore, using **Equations XXXI** and **XXXII**, the TDHSR can be calculated as follows (**Equation XXXIII**):

$$TDHSR = \frac{\sigma_{yt} - \sigma_{xt}}{\sigma_{yt}} = \frac{E(4\nu Z_N \sin^4(\theta) + ((1-\nu)Z_N + (2\nu - 1)Z_T)\sin^2(2\theta))}{\nu(4 + 4\nu + EZ_N(4\sin^4(\theta) - \sin^2(2\theta)) + 2EZ_T \sin^2(2\theta))} \quad \text{(XXXIII)}$$

The tilted transverse isotropy DHSR represents the difference in ratio between the maximum and minimum horizontal principal stresses in a TTI medium. It is a crucial parameter for evaluating shale fracturability and the potential to form a fracture network. When TDHSR is high, hydraulic fracturing tends to generate parallel fractures aligned with the direction of the maximum horizontal principal stress, resulting in non-intersecting fracture planes that hinder shale oil and gas flow. Conversely, when TDHSR is low, hydraulic fracturing can induce fractures in multiple directions, forming an interlaced fracture network that enhances oil and gas migration. Therefore, during fracturing operations, targeting areas with low TDHSR values can help achieve a more effective shale reservoir stimulation.

2.3. Parameter correlation analysis: derivation of the *in situ* stress formula for monoclinic medium

Compared to an HTI medium, which accounts only for the influence of vertical fractures, an OA medium considers both the effect of vertical fractures and the intrinsic anisotropy of the host rock. This intrinsic anisotropy may result not only from the horizontal bedding but also from the inherent anisotropic nature of shale layers or other types of VTI formations. Building on the OA medium, a monoclinic medium further accounts for the fact that fractures are not strictly vertical but are often inclined due to geological structural influences, making it a more realistic representation of actual shale formations. It can be regarded as a result of the combined effects of inclined fractures (which can be considered a TTI medium) and the horizontal bedding of a VTI medium. Therefore, by integrating the linear slip theory and the Bond transformation, the effective compliance tensor, S_m, of the monoclinic medium can be expressed as the sum of the compliance tensor, S_{VTI}, of the VTI medium, which represents the horizontal bedding background, and the compliance tensor, S_f, of inclined fractures after applying the Bond transformation.

The compliance matrix of VTI medium is presented in **Equation XXXIV (see page no 20)**:

The compliance matrix of inclined fractures after Bond transformation $N_\theta S_f N_\theta^T$ is expressed in

Equation XXXV (see page no 20):

According to the Bond transformation, the compliance matrix of a background VTI medium is transformed accordingly. The effective compliance tensor of the monoclinic medium, S_M, can be written as **Equation XXXVI**:

$$S_M = S_{VTI} + N_\theta S_f N_\theta^T \quad \text{(XXXVI)}$$

Substituting the compliance matrix of the monoclinic medium into Hooke's law can result in the matrix presented in **Equation XXXVII**:

$$\begin{bmatrix}\varepsilon_1\\ \varepsilon_2\\ \varepsilon_3\\ \varepsilon_4\\ \varepsilon_5\\ \varepsilon_6\end{bmatrix}=\begin{bmatrix}S_{11m} & S_{12m} & S_{13m} & 0 & S_{15m} & 0\\ S_{21m} & S_{22m} & S_{23m} & 0 & S_{25m} & 0\\ S_{31m} & S_{32m} & S_{33m} & 0 & S_{35m} & 0\\ 0 & 0 & 0 & S_{44m} & 0 & S_{46m}\\ S_{51m} & S_{52m} & S_{53m} & 0 & S_{55m} & 0\\ 0 & 0 & 0 & S_{64m} & 0 & S_{66m}\end{bmatrix}\begin{bmatrix}\sigma_1\\ \sigma_2\\ \sigma_3\\ \sigma_4\\ \sigma_5\\ \sigma_6\end{bmatrix} \quad \text{(XXXVII)}$$

The elements in **Equation XXXVII** are explained in **Equations AI–AXII** in the Appendix A. As in the derivation of the TTI medium formula in the previous text, assuming that there are three principal stresses, the horizontal stresses are not equal, the rock is constrained and cannot move, and the influence of shear stress is ignored. At this time, both the shear stress and the horizontal strain are 0 (**Equations XXXVIII** and **XXXIX**):[34]

$$\varepsilon_x=\varepsilon_1=S_{11m}\sigma_x+S_{12m}\sigma_y+S_{13m}\sigma_z=0 \quad \text{(XXXVIII)}$$

$$\varepsilon_y=\varepsilon_2=S_{21m}\sigma_x+S_{22m}\sigma_y+S_{23m}\sigma_z=0 \quad \text{(XXXIX)}$$

By solving equations through simultaneous equations, the expressions for the horizontal minimum principal stress σ_{xm} and horizontal maximum principal stress σ_{ym} of the monoclinic medium can be obtained through **Equations XL** and **XLI**:

$$\sigma_{xm}=\sigma_z\frac{S_{12m}S_{23m}-S_{13m}S_{22m}}{S_{11m}S_{22m}-S_{12m}^2} \quad \text{(XL)}$$

$$\sigma_{ym}=\sigma_z\frac{S_{12m}S_{13m}-S_{11m}S_{23m}}{S_{11m}S_{22m}-S_{12m}^2} \quad \text{(XLI)}$$

The vertical stress is obtained by integrating the density. Bringing the constant term of the compliance matrix into it yields the corresponding stress expression in **Equations XLII** and **XLIII**:

$$\sigma_{xm}=\sigma_z\left(\begin{array}{l}\left(\begin{array}{l}\sin^2(2\theta)(Z_N-Z_T)\\ \left(\begin{array}{l}M^2(\delta-\varepsilon)-(\delta+1)\mu M+\\ \mu\left(\mu-\sqrt{(M-\mu)(-\mu+2\delta M+M)}\right)\end{array}\right)\\ +2\left(\sqrt{(M-\mu)(-\mu+2\delta M+M)}-\mu\right)\end{array}\right)\\ \hline 2M-\left(\begin{array}{l}M^2(\delta-\varepsilon)-(\delta+1)\mu M+\\ \mu\left(\mu-\sqrt{(M-\mu)(-\mu+2\delta M+M)}\right)\end{array}\right)\\ \left(4Z_N\sin(\theta)^4+Z_T\sin^2(2\theta)\right)\end{array}\right) \quad \text{(XLII)}$$

$$\sigma_{ym}=\sigma_z\frac{\left(\begin{array}{l}\sin^2(2\theta)\left(\begin{array}{l}M^2(\delta-\varepsilon)(Z_N-Z_T)\\ +\mu M(2\gamma-\delta)(Z_N-Z_T)\\ -\mu\left(\sqrt{(M-\mu)(-\mu+2\delta M+M)}-\mu\right)\\ (Z_N-2(\gamma+1)Z_T)\end{array}\right)\\ +2\left(\sqrt{(M-\mu)(-\mu+2\delta M+M)}-\mu\right)\\ +4(2\gamma+1)\mu Z_N\sin(\theta)^4\\ \left(\sqrt{(M-\mu)(-\mu+2\delta M+M)}-\mu\right)\end{array}\right)}{\left(\begin{array}{l}(\delta+1)\mu M-M^2(\delta-\varepsilon)\\ -\mu\left(\mu-\sqrt{(M-\mu)(-\mu+2\delta M+M)}\right)\end{array}\right)\\ \left(4Z_N\sin(\theta)^4+Z_T\sin^2(2\theta)\right)+2M} \quad \text{(XLIII)}$$

The vertical stress can be estimated using seismic or logging data. By integrating the pre-stack wide-azimuth seismic inversion to obtain elastic and anisotropic parameters and then substituting them into **Equations XLII** and **XLIII**, the horizontal minimum principal stress and horizontal maximum principal stress of the monoclinic medium can be predicted. Furthermore, using **Equations XLII** and **XLIII**, the MDHSR can be calculated as follows through **Equation XLIV**:

$$MDHSR=\frac{\sigma_{ym}-\sigma_{xm}}{\sigma_{ym}}$$

$$(2\gamma+1)\mu\left(\begin{array}{l}4Z_N\sin(\theta)^4\\ \left(\mu-\sqrt{(M-\mu)(-\mu+2\delta M+M)}\right)\\ +\sin^2(2\theta)\left(\begin{array}{l}M(Z_T-Z_N)+\\ Z_T\left(\mu-\sqrt{(M-\mu)(-\mu+2\delta M+M)}\right)\end{array}\right)\end{array}\right)$$

$$=\frac{\left(\begin{array}{l}-M^2(\delta-\varepsilon)(Z_N-Z_T)+\mu M(2\gamma-\delta)\\ (-(Z_N-Z_T))+\mu\left(\sqrt{(M-\mu)(-\mu+2\delta M+M)}-\mu\right)\\ (Z_N-2(\gamma+1)Z_T)\end{array}\right)}{2\mu+\sin^2(2\theta)}$$

$$-2\sqrt{(M-\mu)(-\mu+2\delta M+M)}$$

$$-4(2\gamma+1)\mu Z_N\sin(\theta)^4\left(\sqrt{(M-\mu)(-\mu+2\delta M+M)}-\mu\right) \quad \text{(XLIV)}$$

2.4. Verification of the tilted transverse isotropy DHSR

The *in situ* stress formulas for the TTI medium and monoclinic medium derived above must be verified

for their correctness. Therefore, the DHSR formula derived in this paper was compared with the DHSR for the HTI medium and the DHSR for the OA medium. This comparison involved degenerate cases to verify the accuracy of the formulas. Further analysis and verification of the DHSR for the HTI medium, as derived by Gray,[7] are given by the following formula in **Equation XLV**:

$$DHSR = \frac{\sigma_y - \sigma_x}{\sigma_y} = \frac{EZ_N}{1 + EZ_N + \nu} \tag{XLV}$$

The formula for the DHSR of the OA medium derived by Ma *et al.*[11] is presented in **Equation XLVI**:

$$ODHSR = \frac{2V_{S0}^2 \rho (2\gamma + 1) Z_N}{1 + 2V_{S0}^2 \rho (2\gamma + 1) Z_N} \tag{XLVI}$$

Among them, $Z_N = \frac{\delta_N}{M(1 - \delta_N)}$, M = λ + 2μ is the P-wave modulus.

The *in situ* stress formula derived for the TTI medium is based on the anisotropic media theory and establishes the relationship between stress and strain in TTI media through Hooke's law. By applying the assumptions of Iverson's theorem, the *in situ* stress formula expressed in terms of anisotropic and elastic parameters was obtained. Furthermore, the TDHSR was given by **Equation XXXIII**. The TTI medium can be considered as a complex medium obtained by rotating the VTI medium. The elastic matrix of the TTI medium consists of two parts: the isotropic background medium and the anisotropic component caused by fractures. When the inclination angle reached 90°, the strata were considered as an HTI medium. Therefore, by substituting the inclination angle of 90° into the principal stress formula and TDHSR formula derived in this paper, the results matched perfectly with the principal stress formula and DHSR formula of the HTI medium as derived by Gray (**Equation XLVII**). The workflow is illustrated in Figure 3. This comparison fully supports the validity of the *in situ* stress formula for the TTI medium, considering the influence of inclined fractures, as proposed in this paper.

$$\begin{aligned} TDHSR(\theta = 90^\circ) &= \frac{E(4\nu Z_N \sin^4(\theta) + ((1-\nu)Z_N + (2\nu - 1)Z_T)\sin^2(2\theta))}{\nu(4 + 4\nu + EZ_N(4\sin^4(\theta) - \sin^2(2\theta)) + 2EZ_T \sin^2(2\theta))} \\ &= \frac{EZ_N}{1 + EZ_N + \nu} = DHSR \end{aligned} \tag{XLVII}$$

2.5. Verification of the monoclinic DHSR

Following a similar approach to deriving the *in situ* stress formula for the TTI medium, the *in situ* stress formula for the monoclinic medium was derived from the theory of anisotropic media. Using Hooke's law, the relationship between stress and strain in the monoclinic medium was established. According to Iverson's theorem, the *in situ* stress formula, expressed in terms of anisotropic and elastic parameters, was obtained, along with the MDHSR for the monoclinic medium, given by **Equation XLIV**. For the monoclinic medium, it can be regarded as a result of the rotation of the vertical fractures assumed in the OA medium. The elastic matrix of the monoclinic medium consisted of a VTI medium component, representing horizontal strata, and a TTI medium component, representing inclined fractures. As the inclination angle increased, rotation occurred. When the inclination angle θ reached 90°, the medium was regarded as an OA medium. Therefore, by substituting an inclination angle of θ = 90° into the principal stress formula and MDHSR formula of the monoclinic medium derived in this paper, the formula degraded completely, yielding results that matched precisely with the principal stress formula and DHSR formula for the OA medium derived by Ma *et al.*[11] This fully supports the validity of the *in situ* stress formula for the monoclinic medium, considering the combined influence of inclined fractures and horizontal bedding.

Compared to the TTI medium, the monoclinic medium further incorporates the influence of horizontal bedding in strata, in addition to considering the effect of inclined fractures. In the *in situ* stress formula and the MDHSR, both the compliance parameters of the TTI medium (representing fractures) and the anisotropic parameters of the VTI medium (representing horizontal bedding) were present. It can be considered that when the influence of horizontal bedding was ignored in the monoclinic medium, the shale strata degenerated from the monoclinic medium to the TTI medium. To verify the rationality of the formula derived in this paper, we further simplified it by removing the anisotropic parameters from the *in situ* stress and MDHSR formulas of the monoclinic medium. Specifically, the parameters ε, δ and γ were set to zero. This step allowed for a more intuitive assessment of the formula's validity and ensured its broader applicability in practical scenarios. The resulting *in situ* stress and TDHSR formula, obtained after eliminating the anisotropic parameters, are presented in **Equations XLVIII–L**:

$$\sigma_x = \sigma_z \left(\frac{M - 2\mu + (Z_N - Z_T)(\mu - M)\mu \sin^2(2\theta)}{M(M-\mu)\mu\left(4Z_N \sin^4(\theta) + Z_T \sin^2(2\theta)\right)} \right) \quad \text{(XLVIII)}$$

$$\sigma_y = \sigma_z \left(\frac{(M-2\mu)\begin{pmatrix} 2 + 4Z_N \mu \sin^4(\theta) - (Z_N - 2Z_T) \\ \mu \sin^2(2\theta) \end{pmatrix}}{2\left(M + (M-\mu)\mu\left(4Z_N \sin^4(\theta) + Z_N \sin^2(2\theta)\right)\right)} \right) \quad \text{(XLIX)}$$

$$TDHSR = \frac{\mu\begin{pmatrix} 4Z_N \sin(\theta)^4 (M-2\mu) + \sin^2(2\theta) \\ (MZ_N - 2\mu Z_T) \end{pmatrix}}{(M-2\mu)\begin{pmatrix} 4\mu Z_N \sin(\theta)^4 - \mu \sin^2(2\theta) \\ (Z_N - 2Z_T) + 2 \end{pmatrix}} \quad \text{(L)}$$

In the transversely isotropic media, the relationship between the P-wave modulus, the S-wave modulus, the Young's modulus, and the Poisson's ratio can be expressed as follows (**Equations LI** & **LII**):

$$M = \frac{E(1-\nu)}{(1+\nu)(1-2\nu)} \quad \text{(LI)}$$

$$\mu = \frac{E}{2(1+\nu)} \quad \text{(LII)}$$

Substituting this relationship into **Equations XLVIII–L**, with transformations, we obtained **Equations LIII–LV**:

$$\sigma_x = \sigma_z \left(\frac{\upsilon + \upsilon^2 + \frac{1}{4}E(Z_T - Z_N)\sin^2(2\theta)}{1 - \upsilon^2 + EZ_N \sin^4(\theta) + \frac{1}{4}EZ_T \sin^2(2\theta)} \right) \quad \text{(LIII)}$$

$$\sigma_y = \sigma_z \upsilon \left(\frac{\begin{matrix} 1 + \upsilon - EZ_N(\frac{1}{4}\sin^2(2\theta) - \sin^4(\theta)) \\ + \frac{1}{2}EZ_T \sin^2(2\theta) \end{matrix}}{\begin{matrix} 1 - \upsilon^2 + EZ_N \sin^4(\theta) \\ + \frac{1}{4}EZ_T \sin^2(2\theta) \end{matrix}} \right) \quad \text{(LIV)}$$

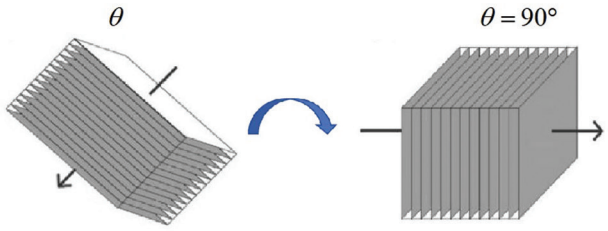

Step 1. $\theta = 90°$ ⟹ $\sin^2(2\theta) = 0 \quad \sin^4(\theta) = 1$

Step 2.

$$\sigma_{xt} = \sigma_z \left(\frac{\upsilon + \upsilon^2 + \frac{1}{4}E(Z_T - Z_N)\sin^2(2\theta(\theta = 90°))}{1 - \upsilon^2 + EZ_N \sin^4(\theta(\theta = 90°)) + \frac{1}{4}EZ_T \sin^2(2\theta(\theta = 90°))} \right) = \sigma_z \upsilon \left(\frac{1+\upsilon}{1 - \upsilon^2 + EZ_N} \right)$$

$$\sigma_{yt} = \sigma_z \upsilon \left(\frac{1 + \upsilon - EZ_N(\frac{1}{4}\sin^2(2\theta(\theta = 90°)) - \sin^4(\theta(\theta = 90°))) + \frac{1}{2}EZ_T \sin^2(2\theta(\theta = 90°))}{1 - \upsilon^2 + EZ_N \sin^4(\theta(\theta = 90°)) + \frac{1}{4}EZ_T \sin^2(2\theta(\theta = 90°))} \right) = \sigma_z \upsilon \left(\frac{1 + \upsilon + EZ_N}{1 - \upsilon^2 + EZ_N} \right)$$

Step 3.

$$\frac{\sigma_{yt} - \sigma_{xt}}{\sigma_{yt}} = \frac{\sigma_z \upsilon \left(\frac{1 + \upsilon + EZ_N}{1 - \upsilon^2 + EZ_N} \right) - \sigma_z \upsilon \left(\frac{1+\upsilon}{1 - \upsilon^2 + EZ_N} \right)}{\sigma_z \upsilon \left(\frac{1 + \upsilon + EZ_N}{1 - \upsilon^2 + EZ_N} \right)} = \frac{EZ_N}{1 + EZ_N + \nu} = DHSR$$

Figure 3. Workflow for converting the tilted transverse isotropy differential horizontal stress ratio to the differential horizontal stress ratio (DHSR)
Note: θ represents the fracture dip angle, E represents the Young's modulus, and v represents the Poisson's ratio. Z_N is the normal compliance tensor of the fracture surface, representing the unit normal displacement (deformation) caused by a unit normal stress. Z_T is the tangential compliance tensor of the fracture surface, representing the unit tangential displacement caused by a unit tangential stress (parallel to the contact surface). Z_N increases with increasing θ. Z_T depends only on 2θ, when $\theta = 90°$, $\sin 2\theta = 0$. Therefore, DHSR is independent of Z_T
Abbreviations: HTI: Horizontally transversely isotropic medium; TTI: Tilted transversely isotropic medium

$$TDHSR = \frac{E(4\nu Z_N \sin^4(\theta) + ((1-\nu)Z_N + (2\nu - 1)Z_T) \sin^2(2\theta))}{\nu(4 + 4\nu + EZ_N(4\sin^4(\theta) - \sin^2(2\theta)) + 2EZ_T \sin^2(2\theta))} \quad \text{(LV)}$$

Equations LIII–LV are consistent with the *in situ* stress and TDHSR formulas (**Equations XXXI–XXXIII**) of the TTI medium derived previously. The consistency of the two was mutually verified through formula degradation, thus proving the correctness of the *in situ* stress formulas of the two complex media derived in this paper.

3. Complex medium *in situ* stress sensitivity analysis

From the research and derivation of the complex medium *in situ* stress formulas presented earlier, it can be concluded that, compared to the DHSR of the HTI and OA media, which are controlled by a limited number of parameters, the TDHSR and MDHSR derived in this paper are influenced by a greater number of factors. To gain a deeper understanding of the *in situ* stress formula, the influence of individual parameters on the TDHSR and MDHSR formulas derived above was further studied through a controlled variable approach.

3.1. Influence of elastic parameters and anisotropic parameters on the tilted transverse isotropy DHSR

Taking the study of the influence of Young's modulus on the TDHSR as an example, assume that the Poisson's ratio of the TTI background medium is ν = 0.35. The Young's modulus increases by 2 GPa at each step, with the range spanning from 20 GPa to 40 GPa. The normal compliance and tangential compliance of fractures are given as Z_N = 2.5×10^{-12} and Z_T = 2.5×10^{-12}, respectively. The fracture dip angle starts at 0° and increases by 10° at each step, with a maximum dip angle of 90°. As the fracture dip angle changes, the influence of Young's modulus on the TDHSR is shown in Figure 4. When the fracture dip angle is 0°, the TTI medium degenerates into a VTI medium. According to Gray's assumption, TDHSR is zero at this point. For a fixed fracture dip angle, as Young's modulus increases, TDHSR shows a positive correlation. In other words, the greater the Young's modulus, the higher the TDHSR. Furthermore, with other parameters held constant, TDHSR exhibited a linear increase as the fracture inclination angle increased.

Following the same approach to study the influence of different parameters on TDHSR, it can be observed that as various parameters increase, TDHSR exhibits either an increasing or decreasing trend. When the stratum dip angle is 0°, TDHSR is zero. As the stratum dip angle increases, TDHSR shows an increasing trend. In particular, for tangential compliance, when the fracture dip angle reaches 90°, TDHSR remains unchanged with variations in tangential compliance. Through the derivation and analysis of the above formula, it can be concluded that when the TTI medium is rotated by 90° to become an HTI medium, the DHSR formula is given by **Equation XLV.** At this point, the tangential compliance term in the formula is eliminated, and the DHSR becomes independent of tangential compliance, resulting in a constant value.

Figure 5 shows the variation of TDHSR under the combined influence of anisotropic and elastic parameters. Taking Figure 5A as an example, TDHSR increased with both normal compliance and Young's modulus. TDHSR is more sensitive to normal compliance. From all the subplots in Figure 5, it can be observed that TDHSR is more sensitive to anisotropic parameters compared to elastic parameters. Consistent with the conclusions of the single-parameter sensitivity analysis, TDHSR increased linearly with the dip angle.

3.2. Influence of elastic parameters and anisotropic parameters on the monoclinic DHSR

Similarly, considering the study of the influence of the P-wave modulus on the MDHSR, assume that the shear wave modulus of the monoclinic background medium is μ = 10 GPa. The P-wave modulus M increases by 5 GPa at each step, with the range spanning from 25 GPa to 45 GPa. The anisotropic parameters are set as ε = 0, δ = 0 and γ = 0, while the normal weakness and tangential weakness of fractures are Δ_N = 0.35 and Δ_T = 0.1, respectively. The fracture dip angle starts at 0° and increases by 10° at each step, with a maximum dip angle of 90°. As the fracture dip angle changes, the influence of the P-wave modulus M on the MDHSR is shown in Figure 6. When the fracture dip angle is 0°, the monoclinic medium degenerates into a VTI medium. According to Gray's assumption, MDHSR is zero at this point. For a fixed fracture dip angle, as the P-wave modulus increases, MDHSR shows a negative correlation, indicating that a greater P-wave modulus results in a smaller MDHSR. With other parameters held constant, MDHSR exhibited a linear increase as the fracture dip angle increased. When the fracture dip angle reached 90°, MDHSR remained unchanged with variations in the P-wave modulus. Through the derivation and analysis of the above formula, it can be concluded that when the monoclinic medium is rotated by 90° to become an OA medium, the DHSR formula is given as **Equation XLVI**. At this point, the P-wave modulus M is eliminated from the formula, and the DHSR becomes independent of the P-wave modulus, resulting in a constant value.

When the dip angle of the ground layer or fracture is 0°, the monoclinic medium simplifies to a VTI medium. According to Gray's assumption, the MDHSR is 0 in this case. When the fracture dip angle remains fixed, the MDHSR exhibits a positive correlation with the anisotropy parameter ε, a negative correlation with the anisotropy parameter δ, and a positive correlation with the anisotropy parameter γ. However, when the fracture dip angle reaches 90°, the MDHSR remains unaffected by the anisotropy parameters.

Following the same approach to studying the influence of different parameters on MDHSR, it can be observed that as various parameters increase, MDHSR exhibits either an increasing or decreasing trend. When the stratum dip angle is 0°, MDHSR remains 0. As the stratum dip angle increases, MDHSR shows an increasing trend. Notably, for P-wave modulus, tangential compliance, and anisotropic parameters, when the fracture dip angle reaches 90°, MDHSR remains unchanged despite variations in these parameters. Through the derivation and analysis of the above formula, it can be concluded that when the monoclinic medium is rotated by 90° to become an OA medium, the DHSR is given in **Equation XLVI**. At this point, the parameter terms in the formula are eliminated, indicating that the DHSR is unaffected by these values and remains a constant.

Figure 7 illustrates the variation of MDHSR under the combined influence of anisotropic and elastic parameters. Taking Figure 7C as an example, MDHSR increases with both normal compliance and S-wave modulus. MDHSR is more sensitive to normal compliance. From all the subplots in Figure 7, it can be observed that MDHSR is more sensitive to anisotropic parameters compared to elastic parameters. Consistent with the conclusions of the single-parameter sensitivity analysis, MDHSR increases linearly with the dip angle.

4. Model example analysis

4.1. Methodology and workflow for *in situ* stress prediction

Based on the previously discussed stress characterization methods for complex media, a stress inversion approach grounded in complex medium theory can ultimately be established. This method primarily consists of five steps.

4.1.1. Seismic data preparation

To invert for the anisotropic parameters used in stress prediction, at least six azimuthal elastic impedance

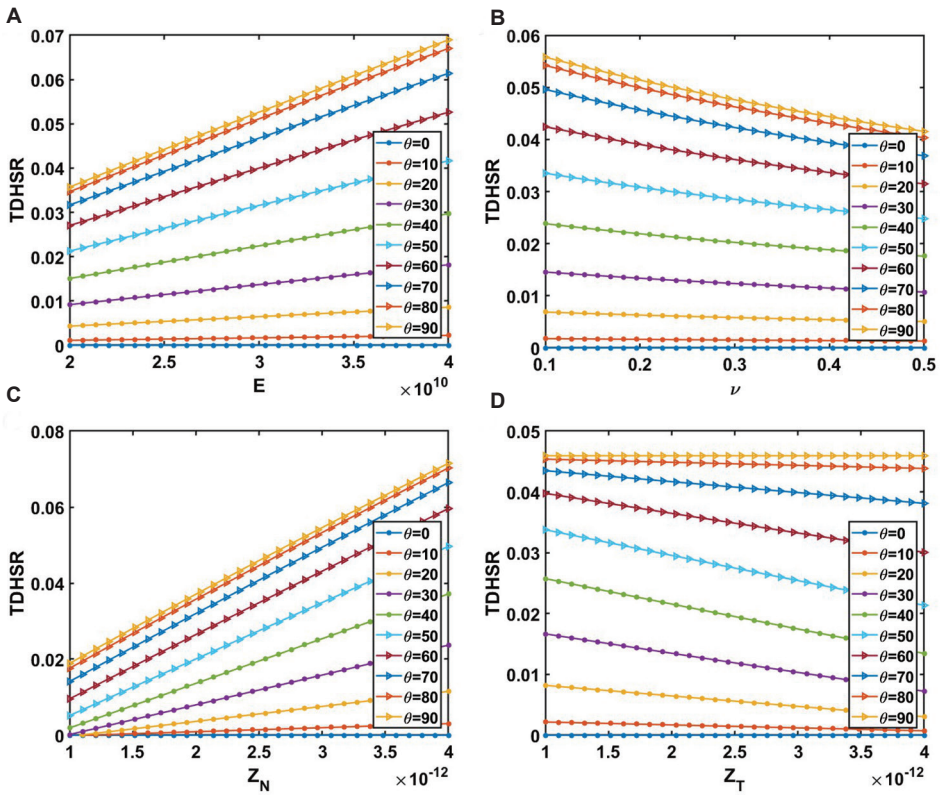

Figure 4. Influence of elastic parameters and anisotropic parameters on the tilted transverse isotropy differential horizontal stress ratio (TDHSR). (A) Young's modulus. (B) Poisson's ratio. (C) Normal compliance. (D) Tangential compliance

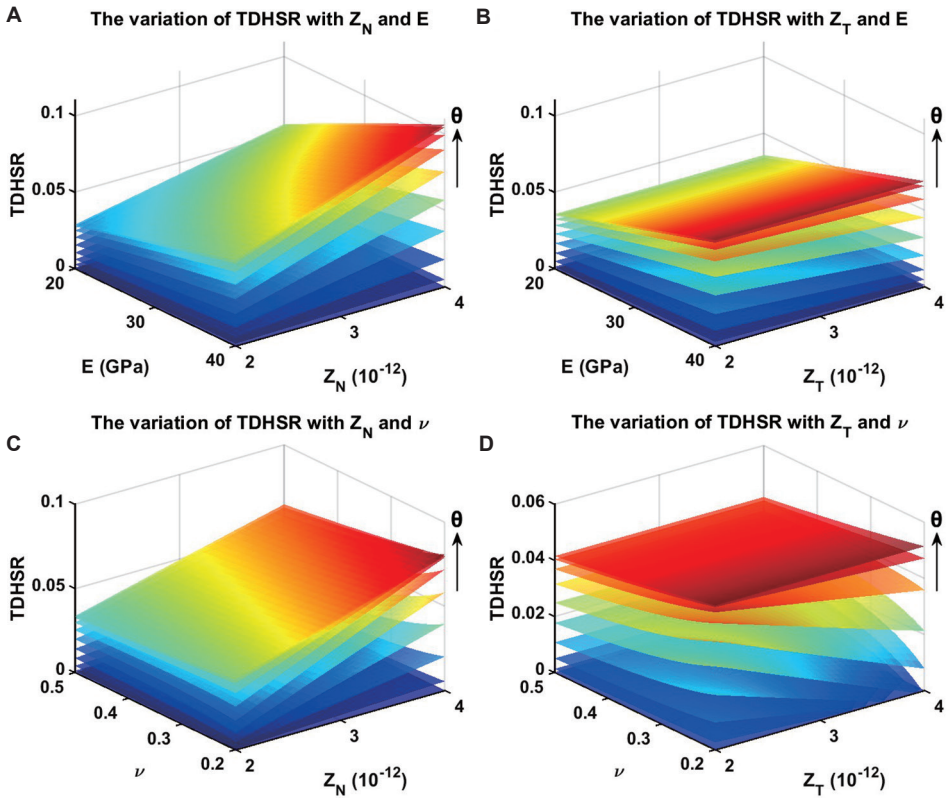

Figure 5. Influence of elastic parameters and anisotropic parameters on the tilted transverse isotropy differential horizontal stress ratio (TDHSR). (A) Normal compliance and Young's modulus. (B) Tangential compliance and Young's modulus. (C) Normal compliance and Poisson's ratio. (D) Tangential compliance and Poisson's ratio

(EI) data volumes are required. The wide-azimuth pre-stack seismic data are divided according to the azimuth rose diagram. Starting from zero degrees, six pre-stack seismic gathers are selected to ensure uniform azimuthal distribution and roughly equal fold coverage. The final selected data consist of six volumes—representing small, medium, and large incidence angles—at the two azimuths with the highest fold coverage.

4.1.2. Azimuthal elastic impedance inversion

Using the six partial-angle stacked seismic volumes, azimuthal EI inversion is performed individually for each volume. By incorporating rock physics information and constraints such as wavelets, well logs, seismic horizons, and low-frequency models, six azimuthal EI volumes are obtained through constrained elastic impedance inversion.

4.1.3. Elastic parameter inversion based on elastic impedance

The six-angle elastic impedance volumes are used as input to derive the complete volumes of P-wave velocity, S-wave velocity, density, and anisotropic parameters within the study area. Fracture compliance parameters can further be obtained through equation-based transformations.

4.1.4. Determination of formation and fracture dip angles

Given that this study focuses on stress prediction in shale formations with bedding or fracture dip (i.e., complex media), it is necessary to determine the dip angle. Due to its low cost and maturity, image logging is typically used to measure and determine the dip of formations and fractures.

4.1.5. Calculation of horizontal stress ratio and stress prediction

Once the elastic parameters, anisotropic parameters, and dip angles of formations and fractures required for stress calculation in complex media are obtained, the previously derived complex medium stress equations—based on linear slip theory, anisotropy theory, and Bond transformation—are used. Ultimately, the prediction of *in situ* stress is achieved by calculating the DHSR, either TDHSR or MDHSR, for complex media.

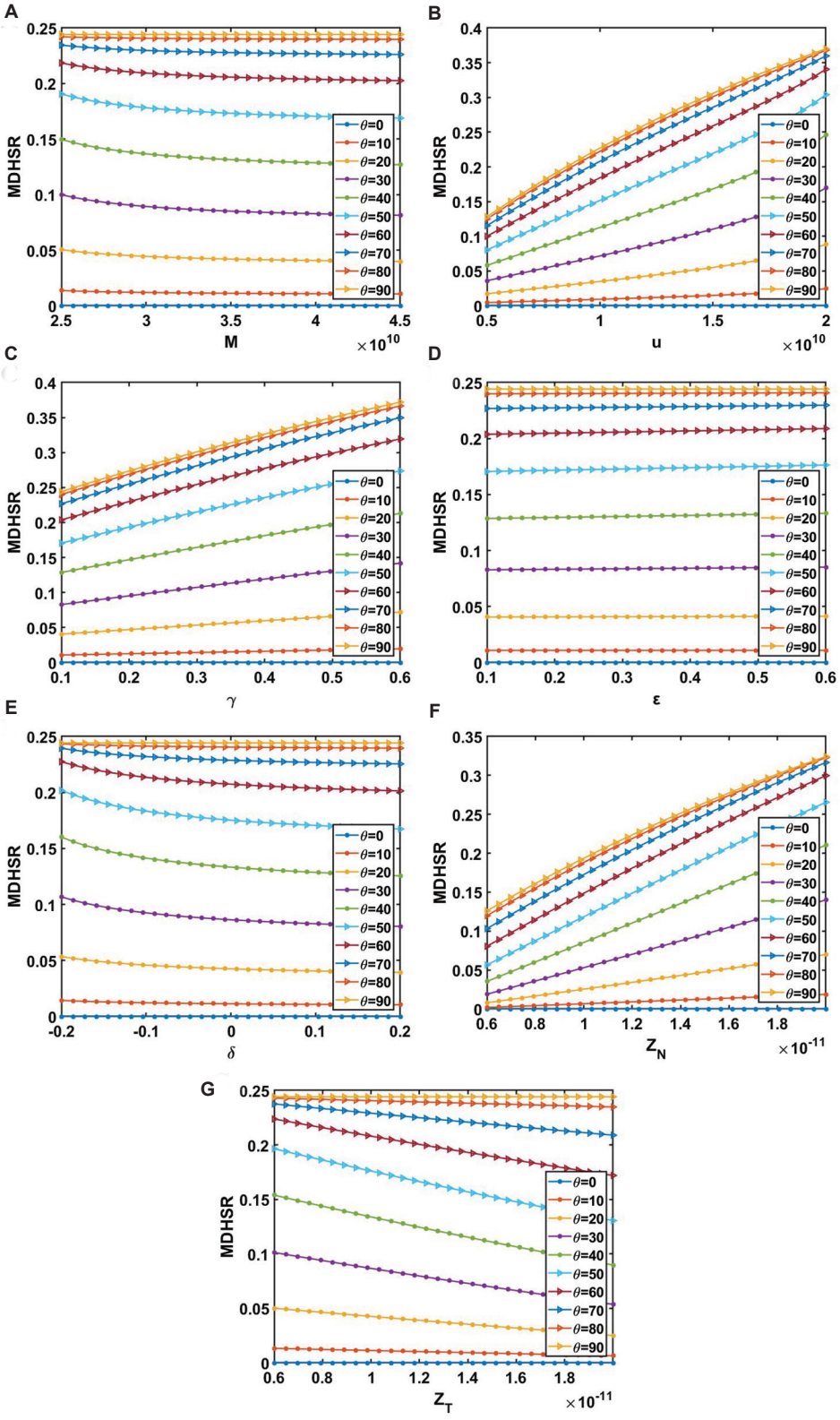

Figure 6. Influence of fracture compliance parameters on the monoclinic differential horizontal stress ratio (MDHSR). (A) P-wave modulus. (B) S-wave modulus. (C) Anisotropic parameter. (D) Anisotropic parameter. (E) Anisotropic parameter. (F) Normal compliance. (G) Tangential compliance

4.2. Field data experiment

To further validate the correctness of the *in situ* stress formula derived in this study, actual logging data must be used for trial calculations. The measured logging curve from Well A, located in the shale formation of the Sichuan Basin, China, was selected for this purpose. A fractured shale formation petrophysical model was constructed to perform the model trial calculations. By inputting measured parameters such as P-wave and S-wave velocities, rock mineral composition, as well as the bulk modulus, shear modulus, and density of each component, along with water saturation and porosity, the anisotropic parameters and fracture compliance parameters required for the *in situ* stress formula were obtained. Figure 8 presents the anisotropic parameters ε, δ, and γ, the fracture normal compliance Z_N, the tangential compliance Z_T, Young's modulus, Poisson's ratio, P-wave modulus M, and S-wave modulus μ for Well A.

The stress measurement point on Well A was selected for model trial calculations. By comparing the DHSR at the measurement point with TDHSR, derived from the TTI medium theory, and MDHSR, derived from the monoclinic medium theory, an error analysis was conducted. Figure 8 presents a comparison of the DHSR at the measured point with TDHSR based on the TTI medium theory, while Figure 9 shows a comparison with MDHSR based on the monoclinic medium theory. As observed in the figures, both TDHSR and MDHSR calculations aligned closely with the measured DHSR, demonstrating the practical applicability of the formula derived in this study. An error analysis was performed on the results, as shown in Table 3, which presents the error analysis of DHSRs at different measurement points. The table indicates that the errors of TDHSR and MDHSR obtained from the model trial calculations fall within a reasonable range. By comparing the errors, it is evident that MDHSR, based on the monoclinic medium theory—which accounts for both horizontal stratification and inclined fractures—exhibited smaller errors and aligned more closely with the measured results than TDHSR, which is based on the TTI medium theory and only considers a single inclined stratum or fracture.

5. Discussion

It is important to acknowledge that the current validation of the TDHSR and MDHSR methods was based on

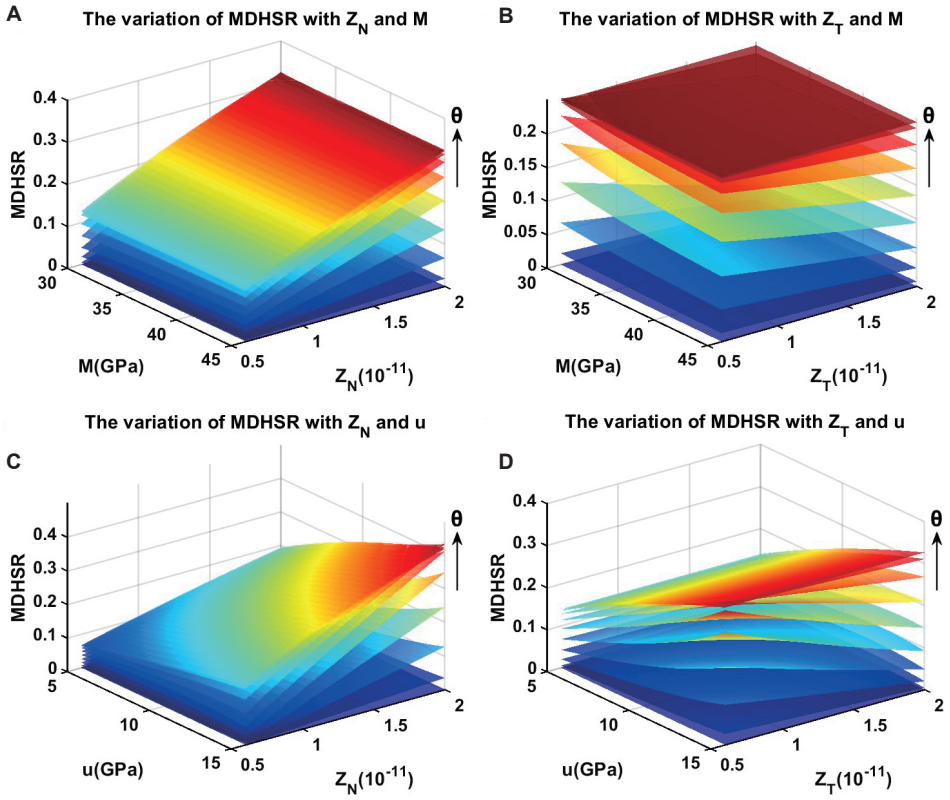

Figure 7. Influence of fracture compliance parameters on the monoclinic differential horizontal stress ratio (MDHSR). (A) Normal compliance and P-wave modulus. (B) Tangential compliance and P-wave modulus. (C) Normal compliance and S-wave modulus. (D) Tangential compliance and S-wave modulus

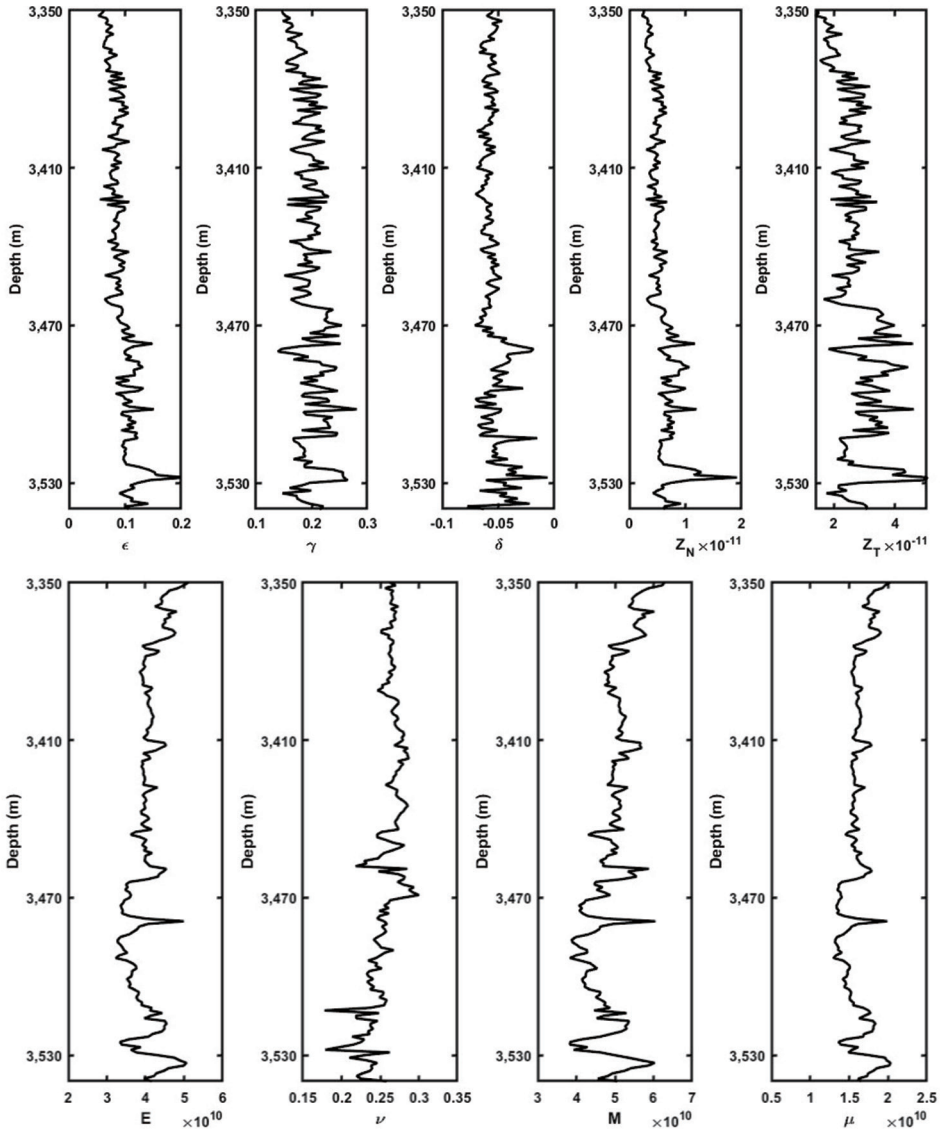

Figure 8. Elastic parameters and anisotropic parameters of Well A

data from a single well in the Sichuan Basin. While the method demonstrated promising accuracy for the studied well, its generalization to other geological settings requires caution. The Sichuan Basin's unique lithology and tectonic history may limit direct extrapolation to basins with differing diagenetic processes or structural complexities.

Future work should consider expanding the application and validation of the proposed methods using data from wells in other basins with diverse geological characteristics. This includes, for example, the Ordos Basin (characterized by stable cratonic settings), the Tarim Basin (with complex deep structures), and foreland basins with strong tectonic deformation. In addition, future work can explore formations with different structural types (e.g., anticlines, fault blocks) and lithologies (e.g., carbonate, sandstone, and tight shale formations). Furthermore, the use of synthetic seismic models and publicly available benchmark datasets should be considered to provide supplementary validation and to better isolate and understand the influence of specific parameters such as fracture dip, azimuthal anisotropy, and stratification. Multi-case verification will enhance the robustness and applicability of the TDHSR and MDHSR approaches, making them more adaptable to various exploration scenarios.

Table 3. Error analysis table of horizontal stress difference ratios at different measured points

Depth (m)	Measured horizontal maximum stress (Mpa)	Measured horizontal maximum stress (Mpa)	Horizontal stress difference ratio	TDHSR	Error	MDHSR	Error
3,483	101.4	86.3	0.149	0.135	9.4%	0.152	2.0%
3,490	102.3	90.5	0.115	0.105	8.7%	0.117	1.7%
3,501	104.6	88.5	0.153	0.141	7.8%	0.146	4.6%
3,508	103.2	88.9	0.139	0.126	9.4%	0.141	1.8%

Abbreviations: MDHSR: Monoclinic differential horizontal stress ratio; TDHSR: Tilted transverse isotropy differential horizontal stress ratio.

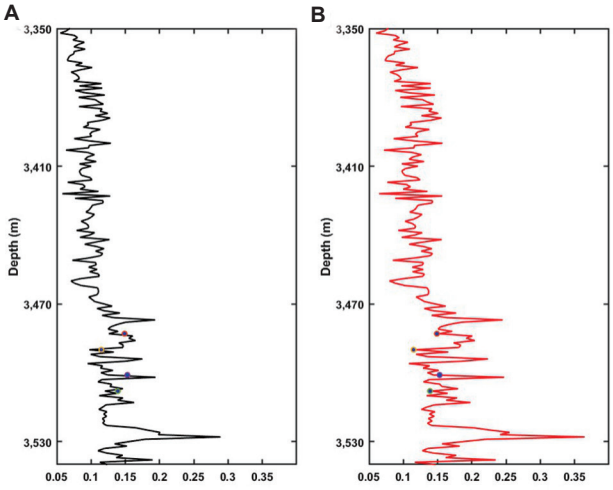

Figure 9. Comparison chart of horizontal stress difference ratio of measured points with the tilted transverse isotropy differential horizontal stress ratio (TDHSR) and the monoclinic differential horizontal stress ratio (MDHSR). (A) TDHSR based on TTI medium theory and (B) MDHSR based on monoclinic medium

6. Conclusion

In situ stress plays a crucial role in the formation and distribution of oil and gas reservoirs. The development and evolution of geological structures result from the action and variation of tectonic stress. The underground stress field influences rock layer deformation, fracture formation, and crack development. For instance, faults are formed due to the fracturing or sliding of strata under *in situ* stress. The type of faults can be assessed based on *in situ* stress prediction results. In addition, the variation of *in situ* stress differs across lithologies, allowing it to serve as an indicator of underground lithology. Therefore, predicting *in situ* stress holds significant research value. A thorough understanding of the *in situ* stress field enables the identification of potential oil and gas accumulation areas, providing essential guidance for exploration efforts.

This paper primarily investigated the seismic prediction method for *in situ* stress based on complex medium theory. It built upon existing seismic prediction methods derived from HTI and OA media while considering the impact of inclined fractures in actual shale formations. By incorporating the assumptions of Schoenberg and Iverson and utilizing the constitutive equation along with coordinate transformations of the elastic matrix, this study derived *in situ* stress formulas for both TTI and monoclinic media, leading to the corresponding DHSRs: TDHSR and MDHSR.

Finally, a model trial calculation was performed using actual logging data from a shale formation. The results demonstrated that the errors of TDHSR and MDHSR remained within a reasonable range. Compared to TDHSR, which was based on the TTI medium and considered only a single inclined stratum or fracture, MDHSR, derived from the monoclinic medium theory, accounted for both horizontal stratification and inclined fractures, leading to smaller errors and results that aligned more closely with the measured data. In conclusion, the TDHSR and MDHSR formulas derived in this study exhibited high accuracy and strong practical applicability.

Acknowledgments

None.

Funding

This research received no external funding.

Conflict of interest

The authors declare no conflicts of interest.

Author contributions

Conceptualization: Jun Cheng, Yaojie Chen
Data curation: Yaojie Chen
Formal analysis: Zhensen Sun
Investigation: Jun Cheng
Methodology: Zhensen Sun
Resources: Jun Cheng
Software: Yaojie Chen
Supervision: Jun Cheng
Validation: Jun Cheng, Zhensen Sun

Writing–original draft: Jun Cheng, Yaojie Chen
Writing–review & editing: Jun Cheng, Yaojie Chen

Availability of data

Due to confidentiality restrictions, the data analyzed in this study cannot be made available to readers.

References

1. Crampin S. The fracture criticality of crustal rocks. *Geophys J Int*. 1994;118(2):428-438.

   doi: 10.1111/j.1365-246X.1994.tb03974.x

2. Yin XY, Cao DP, Wang BL, Zong ZY. Research progress on fluid identification method based on pre-stack seismic inversion. *Oil Geophys Prospect*. 2014;49(1):22-34.

   doi: 10.13810/j.cnki.issn.1000-7210.2014.01.002

3. Du BY, Yang WY, Wang EL, Zhang GZ, Gao J. AVAZ inversion method for fracture media based on young's modulus, poisson's ratio and anisotropy gradient. *Oil Geophys Prospect*. 2015;54(2):218-225.

   doi: 10.3969/j.issn.1000-1441.2015.02.014

4. Zhang GZ, Chen JJ, Chen HZ, Ma GZ, Li CC, Yin XY. Study on *in-situ* stress prediction method based on shale rock physics equivalent model. *Chin J Geophys*. 2015;58(6):2112-2122.

5. Gray FD, Anderson PF, Logel J, Delbecq F, Schmidt D. Estimating *In-Situ*, Anisotropic, Principal Stresses from 3D Seismic. In: *EAGE Conference and Exhibition*; 2010.

6. Gray FD, Anderson PF, Corp A, Logel J, Delbecq F, Schmidt D. *Principle Stress Estimation in Shale Plays using 3D Seismic*. Boca Raton: GeoCanada; 2010.

7. Gray FD. *Methods and Systems for Estimating Stress using Seismic Data*. United States Patent Application no 20110182144A1; 2011.

8. Gray FD, Logel J, Delbecq F, Schmidt D, Schmid R. Estimation of stress and geomechanical properties using 3D seismic data. *First Break*. 2012;30(3):59-68.

   doi: 10.3997/1365-2397.2011042

9. Ruger A. Variation of P-wave reflectivity with offset and azimuth in anisotropic media. *Geophysics*. 1998;63(3):935-947.

   doi: 10.1190/1.1444405

10. Ge ZJ, Li JY, Chen XH, Yu X, Wu JL. TTI medium fracture parameter inversion based on bayesian linear AVAZ. *Chin J Geophys*. 2018;61(7):3008-3018.

    doi: 10.6038/cjg2018L0703

11. Ma N, Yin XY, Sun CY, Zong ZY. *In-situ* stress inversion method based on azimuthal seismic data. *Chin J Geophys*. 2018;61(2):697-706.

12. Ma N, Yin XY, Sun CY, Zong ZY. Seismic prediction method for *in-situ* stress based on orthotropic medium theory. *Chin J Geophys*. 2017;60(12):4766-4775.

13. Wang C. *Research on Pre-Stack Seismic Evaluation Method for Fracturability of Shale Gas Reservoirs*. Qingdao: China University of Petroleum (East China); 2018.

14. Wang C, Song WQ, Lin YH, Zhang YY, Gao QJ, Wei XW. The prediction method of *in-situ* stress based on pre-stack anisotropic parameter inversion. *Geophys Geochem Exploration*. 2020;44(1):141-148.

15. Li L, Zhang GZ. Estimation of fracture parameters and *in-situ* stress parameter based on extended azimuthal elastic impedance. *Chin J Geophys*. 2022;65(8):3172-3185.

16. Wang ZY, Zhang YP, Yang PK, Li SJ. *In situ* stress field inversion based on regularization theory and its applications. *Chin J Underground Space Eng*. 2023;19(2):751-757.

17. Bao T, Burghardt J. A Bayesian approach for *in-situ* stress prediction and uncertainty quantification for subsurface engineering. *Rock Mech Rock Eng*. 2022;55(8):4531-4548.

    doi: 10.1007/s00603-022-02857-0

18. Feng Y, Gao K, Lacasse S. Bayesian partial pooling to reduce uncertainty in overcoring rock stress estimation. *J Rock Mech Geotech Eng*. 2024;16(4):1192-1201.

    doi: 10.1016/j.jrmge.2023.05.003

19. Feng Y, Gao K, Mignan A, Li JW. Improving local mean stress estimation using Bayesian hierarchical modelling. *Int J Rock Mech Min Sci*. 2021;148:104924.

    doi: 10.1016/j.ijrmms.2021.104924

20. Feng Y, Bozorgzadeh N, Harrison JP. Bayesian analysis for uncertainty quantification of *in situ* stress data. *Int J Rock Mech Min Sci*. 2020;134:104381.

    doi: 10.1016/j.ijrmms.2020.104381

21. Moritz OZ, Oliver H. Bayesian quantification and reduction of uncertainties in 3D geomechanical-numerical models. *J Geophys Res Solid Earth*. 2023;128(1):1-23.

    doi: 10.1029/2022JB024855

22. Tonon F, Amadei B, Pan E. Bayesian estimation of rock mass boundary conditions with applications to the AECL underground research laboratory. *Int J Rock Mech Min Sci*. 2001;38(7):995-1027.

    doi: 10.1016/S1365-1609(01)00036-3

23. Leslie JM, Lawton DC. Structural Imaging Below Dipping Anisotropic Layers: Predictions from Seismic Modeling. In: *66th Annual International Meeting, Expanded Abstracts*. United States: SEG; 1996. p. 719-722.

24. Behera L, Tsvankin I. Migration velocity analysis for tilted transversely isotropic media. *Geophys Prospect*. 2009;57:13-26.

    doi: 10.1111/j.1365-2478.2008.00732.x

25. Tsvankin I. Moveout analysis for transversely isotropic media with a tilted symmetry axis. *Geophys Prospect*. 1997;45(3):479-512.

doi: 10.1046/j.1365-2478.1997.380278.x

26. Isaac JH, Lawton DC. A practical method for estimating effective parameters of anisotropy from reflection seismic data. *Geophysics*. 2004;69(3):681-689.

doi: 10.1190/1.1759454

27. Charles S, Mitchell DR, Holt RA, Lin JW, Mathewson J. Data-driven tomographic velocity analysis in tilted transversely isotropic media: A 3D case history from the Canadian foothills. *Geophysics*. 2008,73(5):261.

doi: 10.1190/1.2952915

28. Popov P, Qin G, Bi L, Kang Z, Li J. Multiphysics and multiscale methods for modeling fluid flow through naturally fractured carbonate karst reservoirs. *SPE Reserv Eval Eng*. 2009;12(02):218-231.

doi: 10.2118/105378-PA

29. Maultzsch S, Chapman M, Liu E, Li XY. Modelling and analysis of attenuation anisotropy in multi azimuth VSP data from the Clair field. *Geophys Prospect*. 2007;55:627-642.

doi: 10.1111/j.1365-2478.2007.00645.x

30. Far ME, Wagner D, Hardage B. Fracture parameter inversion for marcellus shale. *Geophysics*. 2014;79(3):55-63.

doi: 10.1190/geo2013-0236.1

31. Li MQ. *Seismic Response Analysis and Parameter Inversion of Monoclinic Media*. Beijing: China University of Geosciences; 2023.

32. Helbig K. *Foundations of Anisotropy for Exploration Seismics*. United Kingdom: Pergamon Press; 1994. p. 22.

33. Tsvankin I. *Seismic Signatures and Analysis of Reflection Data in Anisotropic Media. Society of Exploration Geophysicists*. Netherlands: Elsevier; 2012.

34. Iverson WP. Closure STRESS Calculations in Anisotropic Formations. In: *SPE Low Permeability Reservoirs Symposium, Society of Petroleum Engineers*; 1995.

Equations

$$s_T = \begin{pmatrix} \frac{1}{E}+\mathrm{Zn}\sin^4(\theta)+\frac{1}{4}\mathrm{Zt}\sin^2(2\theta) & -\frac{\nu}{E} & -\frac{\nu}{E}+\mathrm{Zn}\sin^2(\theta)\cos^2(\theta)-\frac{1}{4}\mathrm{Zt}\sin^2(2\theta) & -\frac{\nu}{E} & -\mathrm{Zn}\sin(2\theta)\sin^2(\theta)-\frac{1}{2}\mathrm{Zt}\sin(2\theta)\cos(2\theta) & 0 \\ -\frac{\nu}{E} & -\frac{1}{E} & 0 & 0 & 0 & 0 \\ -\frac{\nu}{E}+\mathrm{Zn}\sin^2(\theta)\cos^2(\theta)-\frac{1}{4}\mathrm{Zt}\sin^2(2\theta) & -\frac{\nu}{E} & \frac{1}{E}+\mathrm{Zn}\cos^4(\theta)+\frac{1}{4}\mathrm{Zt}\sin^2(2\theta) & 0 & -\mathrm{Zn}\sin(2\theta)\cos^2(\theta)+\frac{1}{2}\mathrm{Zt}\sin(2\theta)\cos(2\theta) & 0 \\ 0 & 0 & 0 & \frac{1}{\mu}+\mathrm{Zt}\cos^2(\theta) & 0 & -\mathrm{Zt}\sin(\theta)\cos(\theta) \\ -\mathrm{Zn}\sin(2\theta)\sin^2(\theta)-\frac{1}{2}\mathrm{Zt}\sin(2\theta)\cos(2\theta) & 0 & -\mathrm{Zn}\sin(2\theta)\cos^2(\theta)+\frac{1}{2}\mathrm{Zt}\sin(2\theta)\cos(2\theta) & 0 & \frac{1}{\mu}+\mathrm{Zn}\sin^2(2\theta)+\mathrm{Zt}\cos^2(2\theta) & 0 \\ 0 & 0 & 0 & -\mathrm{Zt}\sin(\theta)\cos(\theta) & 0 & \frac{1}{\mu}+\mathrm{Zt}\sin^2(\theta) \end{pmatrix} \quad \text{(XXII)}$$

$$S_{VTI} = \begin{pmatrix} \frac{c_{11b}c_{33b}-c_{13b}^2}{4c_{66b}\left(c_{11b}c_{33b}-c_{33b}c_{66b}-c_{13b}^2\right)} & \frac{2c_{66b}c_{33b}+c_{13b}^2-c_{11b}c_{33b}}{4c_{66b}\left(c_{11b}c_{33b}-c_{33b}c_{66b}-c_{13b}^2\right)} & \frac{-c_{66b}c_{13b}}{2c_{66b}\left(c_{11b}c_{33b}-c_{33b}c_{66b}-c_{13b}^2\right)} & 0 & 0 & 0 \\ \frac{2c_{66b}c_{33b}+c_{13b}^2-c_{11b}c_{33b}}{4c_{66b}\left(c_{11b}c_{33b}-c_{33b}c_{66b}-c_{13b}^2\right)} & \frac{c_{11b}c_{33b}-c_{13b}^2}{4c_{66b}\left(c_{11b}c_{33b}-c_{33b}c_{66b}-c_{13b}^2\right)} & \frac{-c_{66b}c_{13b}}{2c_{66b}\left(c_{11b}c_{33b}-c_{33b}c_{66b}-c_{13b}^2\right)} & 0 & 0 & 0 \\ \frac{-c_{66b}c_{13b}}{2c_{66b}\left(c_{11b}c_{33b}-c_{33b}c_{66b}-c_{13b}^2\right)} & \frac{-c_{66b}c_{13b}}{2c_{66b}\left(c_{11b}c_{33b}-c_{33b}c_{66b}-c_{13b}^2\right)} & \frac{c_{11b}c_{66b}-c_{66b}^2}{c_{66b}\left(c_{11b}c_{33b}-c_{33b}c_{66b}-c_{13b}^2\right)} & 0 & 0 & 0 \\ 0 & 0 & 0 & \frac{1}{c_{44b}} & 0 & 0 \\ 0 & 0 & 0 & 0 & \frac{1}{c_{44b}} & 0 \\ 0 & 0 & 0 & 0 & 0 & \frac{1}{c_{66b}} \end{pmatrix}_{6\times 6} \quad \text{(XXXIV)}$$

$$N_\theta S_f N_\theta^T = \begin{pmatrix} Z_N\sin^4(\theta)+\frac{1}{4}Z_T\sin^2(2\theta) & 0 & Z_N\sin^2(\theta)\cos^2(\theta)-\frac{1}{4}Z_T\sin^2(2\boldsymbol{\theta}) & 0 & -Z_N\sin(2\theta)\sin^2(\theta)-\frac{1}{2}Z_T\sin(2\theta)\cos(2\theta) & 0 \\ 0 & 0 & 0 & 0 & 0 & 0 \\ Z_N\sin^2(\theta)\cos^2(\theta)-\frac{1}{4}Z_T\sin^2(2\theta) & 0 & Z_N\cos^4(\theta)+\frac{1}{4}Z_T\sin^2(2\theta) & 0 & -Z_N\sin(2\theta)\cos^2(\boldsymbol{\theta})+\frac{1}{2}Z_T\sin(2\theta)\cos(2\theta) & 0 \\ 0 & 0 & 0 & Z_T\cos^2(\theta) & 0 & -Z_T\sin(\theta)\cos(\theta) \\ -Z_N\sin(2\boldsymbol{\theta})\sin^2(\theta)-\frac{1}{2}Z_T\sin(2\theta)\cos(2\theta) & 0 & -Z_N\sin(2\theta)\cos^2(\theta)+\frac{1}{2}Z_T\sin(2\boldsymbol{\theta})\cos(2\theta) & 0 & Z_N\sin^2(2\theta)+Z_T\cos^2(2\theta) & 0 \\ 0 & 0 & 0 & -Z_T\sin(\theta)\cos(\theta) & 0 & Z_T\sin^2(\theta) \end{pmatrix} \quad \text{(XXXV)}$$

Appendix A

The elements in **Equation XXXVII** are explained as follows in **Equations AI–AXII**:

$$S_{11m}=\frac{M^2(\delta-\varepsilon)-(\delta+1)\mu M+\mu\left(\mu-\sqrt{(M-\mu)(-\mu+2\delta M+M)}\right)}{2(2\gamma+1)\mu\left(2M^2(\delta-\varepsilon)+\mu M(2\gamma-2\delta-1)+2\mu\left(\mu-\sqrt{(M-\mu)(-\mu+2\delta M+M)}\right)\right)}+\mathrm{Zn}\sin^4(\theta)+\frac{1}{4}\mathrm{Zt}\sin^2(2\theta) \quad \text{(AI)}$$

$$S_{12m}=\frac{M^2(\varepsilon-\delta)+\mu M(\delta-2\gamma)+\mu\left(\sqrt{(M-\mu)(-\mu+2\delta M+M)}-\mu\right)}{2(2\gamma+1)\mu\left(2M^2(\delta-\varepsilon)+\mu M(2\gamma-2\delta-1)+2\mu\left(\mu-\sqrt{(M-\mu)(-\mu+2\delta M+M)}\right)\right)} \quad \text{(AII)}$$

$$S_{13m}=\frac{-\sqrt{(M-\mu)(M+2M\delta-\mu)}+\mu}{4M^2(-\delta+\varepsilon)+2M(1-2\gamma+2\delta)\mu+4\left(\sqrt{(M-\mu)(M+2M\delta-\mu)}-\mu\right)\mu}+\mathrm{Zn}\sin^2(\theta)\cos^2(\theta)-\frac{1}{4}\mathrm{Zt}\sin^2(2\theta) \quad \text{(AIII)}$$

$$S_{15m}=-\mathrm{Zn}\sin(2\theta)\sin^2(\theta)-\frac{1}{2}\mathrm{Zt}\sin(2\theta)\cos(2\theta) \quad \text{(AIV)}$$

$$S_{22m}=\frac{M^2(\delta-\varepsilon)-(\delta+1)\mu M+\mu\left(\mu-\sqrt{(M-\mu)(-\mu+2\delta M+M)}\right)}{2(2\gamma+1)\mu\left(2M^2(\delta-\varepsilon)+\mu M(2\gamma-2\delta-1)+2\mu\left(\mu-\sqrt{(M-\mu)(-\mu+2\delta M+M)}\right)\right)} \quad \text{(AV)}$$

$$S_{23m}=\frac{-\sqrt{(M-\mu)(M+2M\delta-\mu)}+\mu}{4M^2(-\delta+\varepsilon)+2M(1-2\gamma+2\delta)\mu+4\left(\sqrt{(M-\mu)(M+2M\delta-\mu)}-\mu\right)\mu} \quad \text{(AVI)}$$

$$S_{33m}=\frac{M^2(\delta-\varepsilon)-(\delta+1)\mu M+\mu\left(\mu-\sqrt{(M-\mu)(-\mu+2\delta M+M)}\right)}{2(2\gamma+1)\mu\left(2M^2(\delta-\varepsilon)+\mu M(2\gamma-2\delta-1)+2\mu\left(\mu-\sqrt{(M-\mu)(-\mu+2\delta M+M)}\right)\right)}+\mathrm{Zn}\cos^4(\theta)+\frac{1}{4}\mathrm{Zt}\sin^2(2\theta) \quad \text{(AVII)}$$

$$S_{35m}=-\mathrm{Zn}\sin(2\theta)\cos^2(\theta)+\frac{1}{2}\mathrm{Zt}\sin(2\theta)\cos(2\theta) \quad \text{(AVIII)}$$

$$S_{44m}=\frac{1}{\mu}+\mathrm{Zt}\cos^2(\theta) \quad \text{(AIX)}$$

$$S_{46m}=-\mathrm{Zt}\sin(\theta)\cos(\theta) \quad \text{(AX)}$$

$$S_{55m}=\frac{1}{\mu}+\mathrm{Zn}\sin^2(2\theta)+\mathrm{Zt}\cos^2(2\theta) \quad \text{(AXI)}$$

$$S_{66m}=\frac{1}{(1+2\gamma)\mu}+\mathrm{Zt}\sin^2(\theta) \quad \text{(AXII)}$$

where ε, γ, and δ are Thomsen anisotropy parameters. ε describes the difference in the P-wave velocity between the vertical and horizontal directions, while γ describes the difference in the S-wave velocity between the vertical and horizontal directions. *M* is the longitudinal wave modulus, representing the ratio of axial stress to axial strain under a uniaxial strain condition.